

Regimes of stability of accelerator modes

Rebecca Hihinashvili¹, Tali Olikier¹, Yaniv S. Avizrats¹,
Alexander Iomin¹, Shmuel Fishman¹, Italo Guarneri^{2,3,4}

¹ Department of Physics, Technion, Haifa 32000, Israel

² Centro di Ricerca per i Sistemi Dinamici

Università dell'Insubria a Como, via Valleggio 11, 22100 Como, Italy

³ Istituto Nazionale per la Fisica della Materia, via Celoria 16, 20133 Milano, Italy

⁴ Istituto Nazionale di Fisica Nucleare, Sezione di Pavia, via Bassi 6, 27100 Pavia, Italy

The phase diagram of a simple area-preserving map, which was motivated by the quantum dynamics of cold atoms, is explored analytically and numerically. Periodic orbits of a given winding ratio are found to exist within wedge-shaped regions in the phase diagrams, which are analogous to the Arnol'd tongues which have been extensively studied for a variety of dynamical systems, mostly dissipative ones. A rich variety of bifurcations of various types are observed, as well as period doubling cascades. Stability of periodic orbits is analyzed in detail.

I. INTRODUCTION

Periodic orbits are the backbone of the description of dynamical systems [1, 2, 3], as they enable global understanding of motion in the entire phase space. In the present paper we explore the periodic orbits of the map [4, 5, 6]:

$$\begin{aligned} J_{n+1} &= J_n + \tilde{k} \sin \theta_{n+1} + 2\pi\Omega \quad \text{mod } 2\pi \\ \theta_{n+1} &= \theta_n + J_n \quad \text{mod } 2\pi . \end{aligned} \tag{I. 1}$$

This map will be denoted \mathfrak{M} in this paper. Like all the other maps which are introduced in this paper, it maps the 2-torus onto itself; however, "mod 2π " will always be left understood in all equations which follow. The map \mathfrak{M} reduces to the Standard Map [3] for $\Omega = 0$. When $\tilde{k} = 0$, for each rational value j/p of Ω the map has periodic orbits of period p . For small $\tilde{k} > 0$ such orbits still exist in a range of Ω around j/p . This range of Ω decreases with p . The region in the (\tilde{k}, Ω) phase diagram, where periodic orbits of period p are found, has the shape of a wedge, with the tip on the Ω axis ($\tilde{k} = 0$). This wedge grows wider as \tilde{k} increases,

and intersects other wedges. Furthermore, as \tilde{k} increases more orbits are generated, others lose stability, and an extremely complicated (\tilde{k}, Ω) phase diagram is generated (see Fig. 1 of [4]). The purpose of the present paper is to understand this diagram.

In the case of dissipative systems, this sort of phase diagrams have been studied extensively [7, 8, 9]. The standard sine-circle map [8]:

$$\theta_{n+1} = \theta_n - K \sin(\theta_n) - 2\pi\Omega, \quad (\text{I. 2})$$

is a paradigm in the study of mode-locking for dissipative maps. If $K = 0$ and Ω is a rational number j/p any trajectory of the sine-circle map returns to its initial value (modulo 2π) after p iterations. For $0 < K < 1$, mode-locking is observed; that is, over a range of Ω values around j/p (the *mode-locking interval*) a periodic trajectory with rational winding number j/p *persists*. This periodic orbit attracts all other orbits asymptotically in time, so that all of them eventually acquire this winding number. The widths of the mode-locking intervals are exponentially small in p , and increase with K up to $K = 1$. The regions thus formed in (K, Ω) parameter space, terminating at $K = 0$, $\Omega = j/p$, are known as *Arnol'd tongues* [7, 9]. For $K > 1$ the tongues intersect, stability of orbits is lost, and new orbits are generated. In the same way as the sine-circle map (I. 2) is representative of dissipative systems, the map (I. 1) is representative of area preserving ones. The wedges in the phase space of (I. 1) where the periodic orbits of period p are found will again be referred to as Arnol'd tongues; however, it will be shown that the phase space structure, and the structure of the tongues in particular, is significantly different. This is expected, because orbits of area-preserving maps cannot attract.

The map (I. 1) was obtained in studies of the quantum dynamics of cold atoms, which are kicked by a standing light wave, and are at the same time accelerated by gravity [5, 6, 11, 12]. The gravitational acceleration is proportional to Ω , the strength of the kicking to \tilde{k} , and ϵ is the separation from quantum resonance, which occurs when the ratio between the kicking period and a natural period of the center-of-mass motion of the atoms is an integer. It was shown that ϵ plays the role of Planck's constant, and the limit $\epsilon \rightarrow 0$ (while $\tilde{k} = k\epsilon$ is fixed) is a pseudo-classical limit that is useful to describe the dynamics for small ϵ [5, 6, 10]. In this limit the map (I. 1) was obtained. Its periodic orbits, and the stable islands around them, account for the Quantum Accelerator Modes [5, 6], which were observed experimentally [11, 12, 13].

Compared to that of dissipative systems, the phase diagram of (I. 1) is much more complicated, mainly because overlaps of different tongues occur at arbitrarily small values of \tilde{k} . Therefore, its numerical exploration demands high precision in determining periodic orbits. A property of (I. 1) which proves of decisive help in this task is that (I. 1), like the Standard Map, can be written as a product :

$$\mathfrak{M} = \mathfrak{I}_B \mathfrak{I}_A, \quad (\text{I. 3})$$

where the maps $\mathfrak{I}_A, \mathfrak{I}_B$ are defined as:

$$\begin{aligned} \mathfrak{I}_A : (J, \theta) &\rightarrow (-J, \theta + J) \\ \mathfrak{I}_B : (J, \theta) &\rightarrow (-J + \tilde{k} \sin(\theta) + 2\pi\Omega, \theta). \end{aligned} \quad (\text{I. 4})$$

and are involutions, that is $\mathfrak{I}_A^2 = \mathfrak{I}_B^2 = 1$ (the identity map). If a map has property (I. 3), then the search for its periodic orbits is greatly simplified, if restricted to the class of those orbits which include fixed points of either involution, as we review in detail in Appendix A. This method was applied in [14] for the calculation of the last separating KAM torus of the Standard Map. In the present work this method is used to calculate periodic orbits of (I. 1), both analytically, in the perturbative regime in Sec II, and numerically in other regimes in Sec.III.

Many classic items of the theory of dynamical systems, such as period-doubling cascades, and other bifurcations [1, 2, 3] are met in the study of map (I. 1). In our analysis we have focused on tongues where Ω at the tip (vertex) takes the values 1 (or 0), 1/2 and 1/3. We searched for periodic orbits such that one of their points is a fixed point of one of the involutions. As the boundaries of the tongue are crossed from inside, periodic orbits are annihilated as a result of coalescence of a stable orbit with an unstable one. Near the tip of the tongue j/p the orbits have j and p coprime. As \tilde{k} is increased these become unstable at some stability border where a period doubling bifurcation takes place. The ratio j/p does not change as a result of continuity. This period doubling is followed by a period doubling cascade, which satisfies a characteristic scaling rule of such a route to chaos for area preserving systems, and is universal [15]. Also below the stability border a pitchfork bifurcation of an orbit of period p to two orbits of the same period takes place, resulting in a cusp in the (\tilde{k}, Ω) phase diagram (compare to [7]). The analysis is performed analytically for small \tilde{k} in Sec.II and mostly numerically in Sec. III. Examples of periodic orbits that cannot

be calculated with the involution method are presented in Sec. IV. The involution method is reviewed in Appendix A and various symmetries of the periodic orbits are presented in this Appendix as well as in Appendix B. Properties of Gauss sums and the relation to points on periodic orbits are outlined in Appendix C. The numerical method for finding periodic orbits is presented in Appendix D and a Hopf bifurcation is examined analytically in Appendix E. As tongues intersect, there are regions in the (\tilde{k}, Ω) phase diagram where orbits characterized by different j/p coexist. These orbits are found in different parts of the (θ, J) phase space, and typically do not "interact".

Here we are interested mainly in stable periodic orbits. If the issue of stability is ignored, strong rigorous results can be obtained. In particular, work by T. Oliner and B. Wajnryb [16] implies that if a line in the tongue (p_1, j_1) starts from its tip (vertex) and intersects the boundary of a tongue (p_2, j_2) which is its Farey neighbor [4,17-19], then it intersects along the way all the tongues (\tilde{p}, \tilde{j}) which are in the interval $[\frac{j_1}{p_1}, \frac{j_2}{p_2}]$, intersecting all its Farey neighbors in the correct order. The same work also suggests that in the center of the tongue (j, p) all the orbits of period $p \cdot l$ (l integer) exist, and their winding number is j/p .

II. PERTURBATIVE CALCULATION OF PERIODIC ORBITS

In this section the periodic orbits of the map (I. 1) are calculated to the first order in \tilde{k} . Throughout this section J_n and θ_n are understood to be on the 2π torus, notably they are taken mod 2π ; moreover, Ω is also taken mod 1. First we note that the n -th iterate of the map (I. 1) at zeroth order in \tilde{k} is:

$$\begin{aligned} J_n &= J_0 + 2\pi\Omega n \\ \theta_n &= \theta_0 + \sum_{n'=0}^{n-1} J_{n'} = \theta_0 + J_0 n + \pi\Omega n(n-1). \end{aligned} \quad (\text{II. 1})$$

In order to determine J_n at the 1st order in \tilde{k} , only the 0-th order in θ is required, and so, on substituting the 2nd eq. of (II. 1) in (I. 1), and iterating n times, we find:

$$J_n = J_0 + \tilde{k} \sum_{n'=1}^n \sin[\theta_0 + (J_0 - \pi\Omega)n' + \pi\Omega n'^2] + 2\pi\Omega n. \quad (\text{II. 2})$$

Substitution of this equation in the second equation of (I. 1) yields

$$\theta_n = \theta_0 + J_0 n + \pi\Omega n(n-1) + \tilde{k} \sum_{n'=1}^n (n-n') \sin[\theta_0 + (J_0 - \pi\Omega)n' + \pi\Omega n'^2]. \quad (\text{II. 3})$$

For a periodic orbit of period p the following equalities hold:

$$\begin{aligned}\theta_p - \theta_0 &= 2\pi s \\ J_p - J_0 &= 2\pi j,\end{aligned}\tag{II. 4}$$

where the integers s and j are the winding numbers of θ and J around the torus. At the 0-th order in \tilde{k} ,

$$\Omega = \frac{j}{p}\tag{II. 5}$$

must hold, and so periodic orbits can be found only for rational values of Ω . For *nonvanishing* \tilde{k} , periodic orbits can be found in an interval around each rational value of Ω . In what follows we solve for periodic orbits for small \tilde{k} , assuming that $(\Omega - \frac{j}{p})$ is also small (this assumption will be verified *a posteriori*). Therefore we replace Ω by $\frac{j}{p}$ in the terms that are proportional to \tilde{k} in (II. 2) and (II. 3).

In order to find a periodic orbit of period p , we seek for a point (θ_0, J_0) which is at once a point in this orbit and a fixed point of one of the involutions (I. 4) (Appendix A). The fixed points of \mathfrak{I}_A satisfy

$$J_0 = 0\tag{II. 6}$$

while the fixed points of \mathfrak{I}_B satisfy

$$J_0 = \frac{1}{2}\tilde{k} \sin \theta_0 + \pi\Omega\tag{II. 7}$$

or

$$J_0 = \frac{1}{2}\tilde{k} \sin \theta_0 + \pi\Omega + \pi.\tag{II. 8}$$

Since the periodic orbits of the map \mathfrak{M} of (I. 1) are identical to those of its inverse, we find in Appendix B that if in a periodic orbit of \mathfrak{M} there is a point with momentum J_i , then in a periodic orbit of this map, not necessarily the same one, there is also a point with momentum $-J_i$. If there is only *one* periodic orbit which is stable (or unstable), then the corollary at the end of Appendix B implies that for each point with momentum J_i there is also one with momentum $-J_i$ in this orbit, and so if p is odd then $J_0 = 0$ is in this periodic orbit. Therefore J_0 of (II. 6) is in a periodic orbit of odd period p . On the other hand, for even p , (II. 7) or (II. 8) is in the periodic orbit. This is discussed in Appendix A.

From (II. 2) and (II. 4) we find that in the leading order in \tilde{k} (or ϵ) a point on a periodic orbit of period p satisfies

$$2\pi\left(\frac{j}{p} - \Omega\right) = \frac{1}{2i} \frac{\tilde{k}}{p} \left\{ \left(e^{i\theta_0} \sum_{n'=1}^p e^{i\pi \frac{j}{p} [(\chi_p-1)n' + n'^2]} \right) - c.c. \right\} \quad (\text{II. 9})$$

where $\chi_p = 0$ for odd p , where (II. 6) holds, while $\chi_p = 1$ for even p where (II. 7) holds and $\chi_p = 1 + p/j$ where (II. 8) holds. We will solve equation (II. 9) for θ_0 to the first order in \tilde{k} and then show that it is consistent with (II. 3) in this order.

For this purpose it is instructive to use properties of Gauss sums [4, 20, 21, 22, 23]. We consider

$$G(p, j) = \sum_{m=1}^p e^{i\pi \frac{j}{p} [(\chi_p-1)m + m^2]} \quad (\text{II. 10})$$

which can be summed ([20, 21, 22, 23], see Eq. (36) of [4]) to give

$$G(p, j) = \sqrt{p} e^{i\xi(j, p)} \quad (\text{II. 11})$$

where $\xi(j, p)$ is real (see Appendix C). Substitution in (II. 9) leads to

$$2\pi \left(\frac{j}{p} - \Omega \right) = \frac{\tilde{k}}{\sqrt{p}} \sin \vartheta \quad (\text{II. 12})$$

where

$$\vartheta = \theta_0 + \xi(j, p). \quad (\text{II. 13})$$

A θ_0 that belongs to a periodic orbit must satisfy this equality.

The Gauss sum (II. 10) also satisfies (this is a corollary of Eqs. (34) and (35) of [4])

$$\sum_{m=1}^p m e^{i\pi \frac{j}{p} [(\chi_p-1)m + m^2]} = \begin{cases} \frac{p+1}{2} G(p, j) & p \text{ odd} \\ \frac{p}{2} (G(p, j) + 1) & p \text{ even} \end{cases}. \quad (\text{II. 14})$$

Substitution in (II. 3) for $n = p$, where p is odd, and using (II. 4) results in:

$$2\pi \left[\frac{s}{p} - \frac{\Omega}{2} (p-1) \right] = \frac{\tilde{k}}{\sqrt{p}} \frac{p-1}{2} \sin \vartheta. \quad (\text{II. 15})$$

It is easy to see that it is consistent with (II. 12) for $s = \frac{j(p-1)}{2}$. For even p one finds in a similar way that

$$2\pi \left[\frac{s}{p} - \frac{\Omega}{2} p \right] = \frac{\tilde{k} \sqrt{p}}{2} \sin \vartheta \quad (\text{II. 16})$$

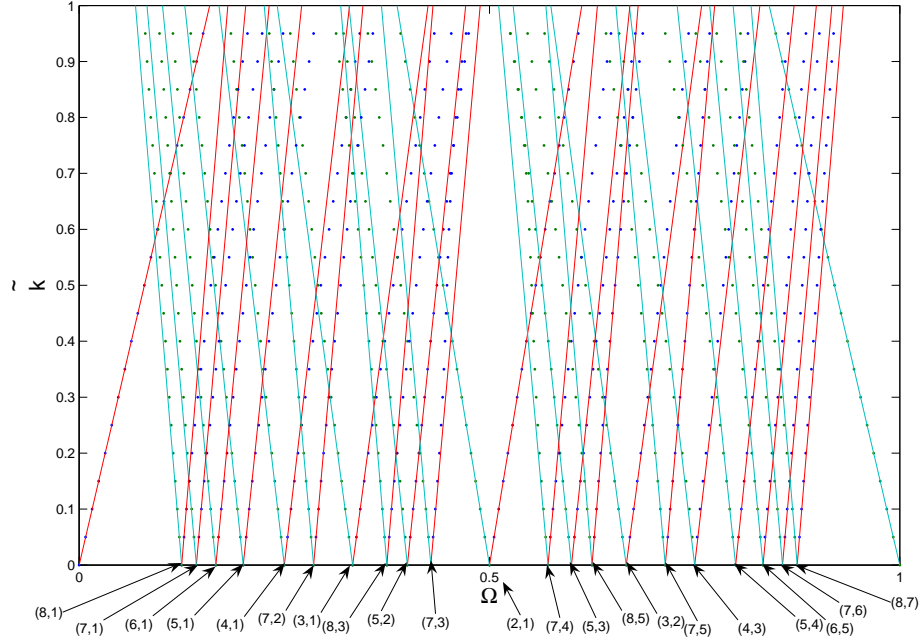


FIG. 1: Various tongues, marked by (p, j) , in the \tilde{k}, Ω phase diagram. For small \tilde{k} the numerical results (dots) coincide with the analytically determined tongue boundaries (solid lines).

and consistency with (II. 12) is possible for $s = \frac{pj}{2}$. Equation (II. 12) determines the periodic orbits in small \tilde{k} . One finds solutions in the range

$$\left| \frac{j}{p} - \Omega \right| \leq \frac{\tilde{k}}{2\pi\sqrt{p}}. \quad (\text{II. 17})$$

This region has the form of a wedge and for small \tilde{k} its boundaries are the lines

$$\Omega = \frac{j}{p} \pm \frac{\tilde{k}}{2\pi\sqrt{p}}, \quad (\text{II. 18})$$

and they are presented in Fig. 1.

Each tongue is characterized by p and j . The inequality (II. 17) justifies our assumption that $|\frac{j}{p} - \Omega|$ is at most of order \tilde{k} (or ϵ). We see that indeed for small \tilde{k} the boundaries are well described by (II. 18). The point ϑ on the orbit is given by (II. 12). Special points are the two in the center of the tongue $\vartheta = 0, \pi$ and the two on its boundaries $\vartheta = \frac{\pi}{2}, \frac{3}{2}\pi$. Since $\xi(j, p)$ is known, one can determine θ_0 from ϑ , as will be shown in Appendix C (see table II). The specific values of θ_0 are of no importance for discussion in the rest of this section, since all the results may be expressed in terms of ϑ . In the regime of small \tilde{k} , for each value of \tilde{k} and Ω there are two periodic orbits, one is stable and the other is unstable. The two

get closer and closer as the boundary is approached and coalesce at the tongue boundaries. We tested numerically the validity of (II. 12) for small \tilde{k} .

The stability of an orbit can be determined as usual from the tangent map. The tangent map of (I. 1) is

$$T(\theta) = \begin{pmatrix} 1 + \tilde{k} \cos \theta & \tilde{k} \cos \theta \\ 1 & 1 \end{pmatrix} \quad (\text{II. 19})$$

and the tangent map over p iterates along a period- p orbit (also termed Monodromy matrix) is given by

$$T_p(\theta_0) = \prod_{i=0}^{p-1} T(\theta_i) . \quad (\text{II. 20})$$

A periodic orbit is stable if

$$|\text{Tr}[T_p(\theta_0)]| < 2 \quad (\text{II. 21})$$

and unstable if the opposite inequality holds. In order to calculate the product (II. 20) to the first order in \tilde{k} we note that (II. 19) can be decomposed as

$$T(\theta_i) = \bar{T}_0 + \tilde{k}\bar{T}_1(\theta_i) \quad (\text{II. 22})$$

where

$$\bar{T}_0 = \begin{pmatrix} 1 & 0 \\ 1 & 1 \end{pmatrix} \quad (\text{II. 23})$$

and

$$\bar{T}_1(\theta_i) = \begin{pmatrix} \cos \theta_i & \cos \theta_i \\ 0 & 0 \end{pmatrix} . \quad (\text{II. 24})$$

With the help of the identities $\text{Tr}(A+B) = \text{Tr}A + \text{Tr}B$ and $\text{Tr}(AB) = \text{Tr}(BA)$ we find that, up to first order in \tilde{k}

$$\text{Tr}(T_p(\theta_0)) = \text{Tr}\bar{T}_0^p + \tilde{k} \sum_{i=1}^p \text{Tr}(\bar{T}_0^{(p-1)}\bar{T}_1(\theta_i)) . \quad (\text{II. 25})$$

It is easy to see that

$$\bar{T}_0^p = \begin{pmatrix} 1 & 0 \\ p & 1 \end{pmatrix} \quad (\text{II. 26})$$

and

$$\bar{T}_1(\theta_i)\bar{T}_0^{(p-1)} = \begin{pmatrix} p \cos \theta_i & \cos \theta_i \\ 0 & 0 \end{pmatrix} . \quad (\text{II. 27})$$

Using (II. 10),(II. 11), and the fact that the angles along a periodic orbit are given to the zeroth order in \tilde{k} by the 2nd equation in (II. 1), one finds that

$$\text{Tr}(T_p(\theta_0)) = 2 + \tilde{k}p^{3/2} \cos \vartheta \quad (\text{II. 28})$$

where ϑ is related to θ_0 by (II. 13).

At the boundaries of the tongue given by (II. 18) the stable and unstable orbits coalesce and $\text{Tr}(T_p(\theta_0)) = 2$. Inside the tongue the orbits with $\frac{\pi}{2} < \vartheta < \frac{3}{2}\pi$ are stable and the ones in the other part are unstable. This was numerically tested.

III. NUMERICAL ANALYSIS OF PERIODIC ORBITS AND STABILITY BORDERS

In the previous section the \tilde{k}, Ω phase diagram was analyzed in the framework of perturbation theory for small \tilde{k} . This approach is valid near the tip of a tongue. In this section the phase diagram is studied in the non-perturbative region. In this region, the edges of a tongue deviate from the straight lines (II. 18) (except in the case $p = 1$, where (II. 18) is exact). Furthermore, this region is characterized by instabilities and bifurcations, which are observed as \tilde{k} is increased. We numerically explore this behavior for some low-period tongues.

As periodic orbits coalesce at the edges of a tongue, their precise numerical determination is difficult near the edges; and this, in turn, makes the precise determination of the edges themselves somewhat delicate. An algorithm we have developed to locate the boundary is presented in Appendix D. From (II. 12) one finds that if ϑ_s and ϑ_u belong to the stable and unstable orbits respectively, then, in the vicinity of the boundary, and for small \tilde{k} ,

$$(\vartheta_u - \vartheta_s)^2 = 16\pi\sqrt{p}\frac{|\delta\Omega|}{\tilde{k}} \quad (\text{III. 1})$$

where $\delta\Omega$ is the distance from the boundary in Ω . This equation can be used to check consistency of results.

The region of existence of a *stable* (j/p) orbit is bounded on the left and on the right by the edges of the tongue, and from above by a stability border, which lies in the interior of the tongue (see, e.g. Fig. 2). Whereas at the edges of the (j/p) tongue, period p orbits, whether stable or unstable, disappear, at the stability border stable periodic orbits become

unstable, and, in the cases considered in this work, a period-doubling cascade follows. Loss of stability is foreshadowed by the perturbative equation (II. 28), because the second term in it is negative for the stable orbit, and so it would lead to violation of (II. 21), and hence to instability, for $|\tilde{k}p^{3/2}\cos(\vartheta)| > 4$. According to this argument, the location of the stability boundary in \tilde{k} decreases with the period as $p^{-3/2}$ (in agreement with earlier work [4]). However, this instability occurs for relatively large values of \tilde{k} , where perturbation theory is no longer valid, and therefore (II. 28) may just provide hints there. In particular, it suggests that stable regions are more likely to be found close to the margins of a tongue, where $\cos(\vartheta)$ is small. This is indeed observed in numerical results: as \tilde{k} increases, the stability border asymptotically approaches the edges of the tongue.

All periodic orbits which are calculated in this section are found by the involution method, which is described in Appendix A. As explained in Appendix D, they are numerically found from the requirement that one point in the orbit is a fixed point of an involution. In the case of odd period p , this is involution \mathfrak{J}_A of (I. 4); for even p , it is typically \mathfrak{J}_B of (I. 4).

A. The tongue $j = 1, p = 1$.

For this tongue many results are known analytically, and were presented in [5, 6, 10]. In particular the boundary of the tongue, and the stability border satisfy ([6], Eq. (32)):

$$\tilde{k}_b = 2\pi|\Omega - 1|, \quad (\text{III. 2})$$

$$\tilde{k}_s = \sqrt{16 + 4\pi^2(\Omega - 1)^2}. \quad (\text{III. 3})$$

These are shown in Fig. 2 along with numerically obtained data (the latter are shown in order to check consistency of our numerical method of finding the boundary). As \tilde{k} increases beyond \tilde{k}_s a period doubling bifurcation takes place, such that the period 1 orbit turns unstable and a period 2 stable periodic orbit appears. Around the $p = 2$ orbit a resonant orbit of period $2 \cdot 3$ is formed, as is shown in Fig. 4 for the case marked by a circle in Fig.2. This mechanism is discussed in Appendix E. For $\Omega = 1$, $\tilde{k} = 2\pi$ a pitchfork bifurcation of the $p = 2$ orbit into two $p = 2$ orbits takes place. The regions where such orbits exist are bound by dashed lines in Fig.2. They are magnified in Fig. 3 and described in detail in the corresponding caption.

The bifurcation which is observed on crossing the stability border upwards is actually the 1st in a period-doubling cascade (marked in Fig. 2 at $\Omega = 1.3692$ by rhombi). Let us denote

by $\delta\theta_n$ the difference in θ between the points separated by half a period in the orbit of period $2^n p$, when it becomes unstable; p is the original period at the start of the period-doubling cascade. We follow the cascade up to $n = 4$ and find that the numerical results as n increases are consistent with:

$$\tilde{k}_n - \tilde{k}_\infty \sim \frac{1}{\delta^n} \quad (\text{III. 4})$$

$$\delta\theta_n \sim \frac{1}{\alpha^n} \quad (\text{III. 5})$$

where \tilde{k}_n are values of \tilde{k} where the $(n + 1)$ -th bifurcation is observed. Estimates for δ and α are reported in Table I, which summarizes this sort of estimates for other tongues as well. \tilde{k}_∞ was calculated using the ratio between the LHS of (III. 4) for n with the one for $n + 1$, thus eliminating the proportionality coefficient. The scaling factors δ and α are universal numbers for the period-doubling route to chaos, in area preserving systems with 2-dimensional phase space. The theoretical prediction of the renormalization group treatment is $\delta \approx 8.721$ $\alpha \approx -4.018$ [15].

B. The tongue $j = 1, p = 2$.

The structure of this tongue is presented in Figs. 5 and 6. First we study the phase portrait at the center of the tongue ($\Omega = 1/2$) for various values of \tilde{k} . For $\tilde{k} = 3.0$ (marked by "o" in Fig. 5), which is below the stability line, the phase portrait is presented in Fig. 7 (2nd and 3d slice from top). In the upper slice, the function $F_\theta(\theta_0)$ is plotted, the zeros of which are used to locate θ_0 of periodic orbits according to the Involution method, as explained in Appendix D. A similar analysis was performed for all periodic orbits. As we increase \tilde{k} , but keep it lower than the stability border \tilde{k}_s , a new stable orbit of period two appears at $\tilde{k} \geq \pi$. Further bifurcations are found for $\tilde{k} > \pi$, and these are described in Fig. 6.

The bifurcation leading from one stable period-2 orbit to two distinct stable orbits with period 2, which is numerically observed at $\tilde{k} = \pi$, is easily obtained analytically. It is a standard pitchfork bifurcation. To see this, we iterate the map (I. 1) twice. The condition for a period two orbit (modulo 2π) is

$$\tilde{k} \sin \theta_0 + \tilde{k} \sin \left(\theta_0 + \frac{\tilde{k}}{2} \sin \theta_0 + \frac{\pi}{2} \right) = 0, \quad (\text{III. 6})$$

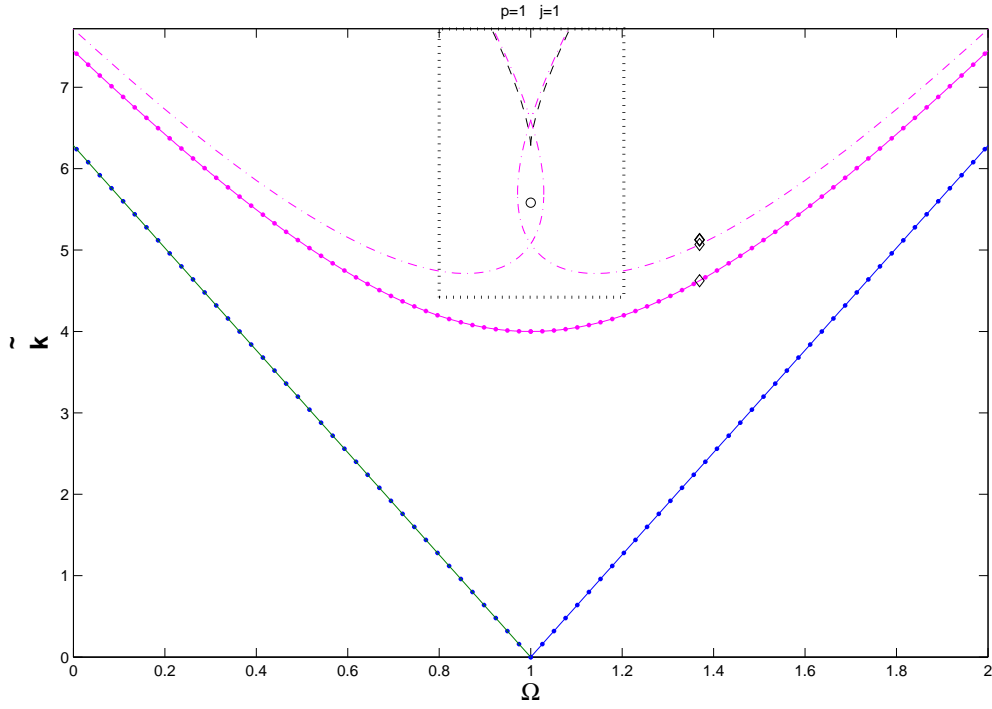


FIG. 2: Phase diagram of the $(j = 1, p = 1)$ tongue. Full lines show the analytical edges of the tongue (straight lines emanating from the point marked by 1 on the horizontal axis) and the analytical stability border of period 1 orbits. Superimposed dots show numerical results. The meaning of symbols (circle, rhombi) is explained in the text. The dash-dotted line marks the stability border of the $p = 2$ orbit which emerges at the period doubling of the $p = 1$ orbit. The region delimited by the dotted-line rectangle is described in Fig. 3.

where $\Omega = 1/2$ and (II. 7) were used. When $\tilde{k} \leq \pi$ there is one stable trajectory. At $\tilde{k} = \pi$, this trajectory is $\{(\pi/2, \pi), (3\pi/2, \pi)\}$ and is marginally stable (the trace of the linearized map $\text{Tr}[T_2(\theta_0)] = 2$). When $\tilde{k} = \pi + \delta\tilde{k}$, two new stable trajectories emerge. To find these zeros of Eq. (III. 6) we replace $\theta_0 = \pi/2 + \delta\theta_0$ and neglect terms of order of $O(\delta\tilde{k}\delta\theta_0^2) \sim O(\delta\theta_0^4)$ and higher. This yields the following cubic equation for $\delta\theta_0$:

$$\delta\theta_0 \cdot \left(\sqrt{\frac{2\delta\tilde{k}}{\pi}} + \delta\theta_0 \right) \cdot \left(\sqrt{\frac{2\delta\tilde{k}}{\pi}} - \delta\theta_0 \right) = 0. \quad (\text{III. 7})$$

The same equation is obtained from the substitution $\theta_0 = 3\pi/2 + \delta\theta_0$. Eq. (III. 7) yields three periodic orbits with period 2. One of them has $\delta\theta_0 = 0$. It continues the unique

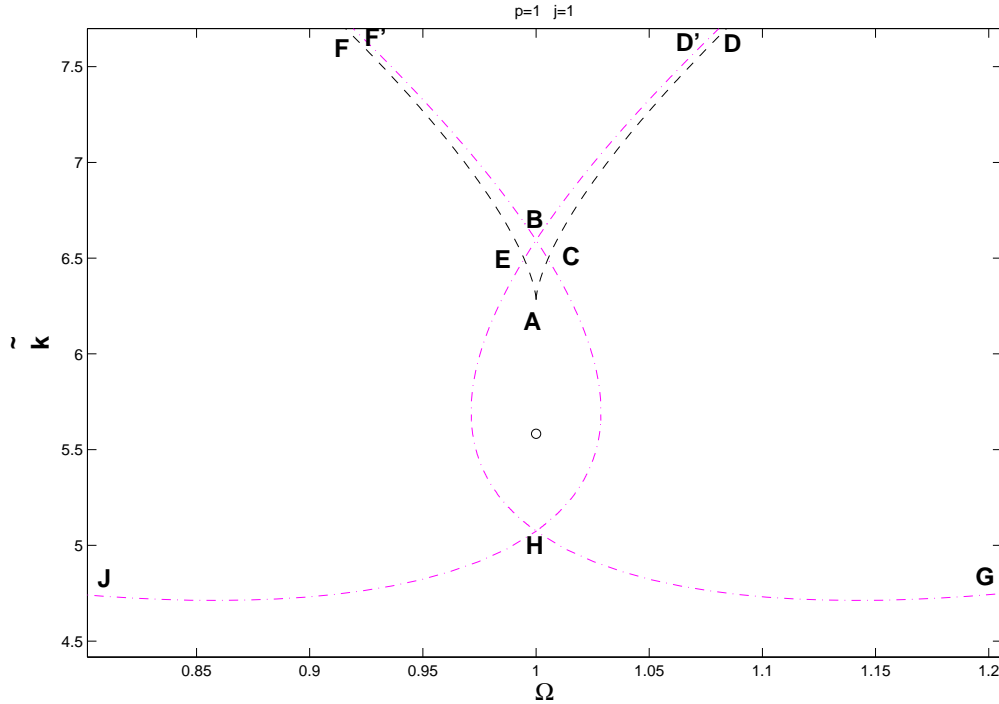


FIG. 3: A zoom-in of the region delimited by the rectangle in Fig. 2. Stable period 2 orbits are found below the line JHG and inside the loop BHB, as well as between the lines EF and BF', and between BD' and CD. Inside the kite-shaped region AEBC, two stable orbits of period 2 are found. A very complicated behaviour is found in the vicinity of H where period 2 and period 4 stable orbits coexist.

orbit at $\tilde{k} = \pi$ and, like that orbit, it is marginally stable *at this order*; numerically, it was found that it is actually unstable, and that $0 \neq \delta\theta_0 = o(\delta\tilde{k})$. The other two orbits have $\delta\theta_0 = \pm\sqrt{\frac{2\delta\tilde{k}}{\pi}}$. They are stable at this order, sharing the same value of $\text{Tr}[T_2] = 2 - 2\pi\delta\tilde{k}$, and are numerically found to be really stable.

On further moving upwards along the axis of the tongue (that is, increasing \tilde{k} while $\Omega = 1/2$), the two period-2 stable orbits persist until point *B* is reached. There they turn unstable, and give rise to two stable period-4 orbits. Two stable period-2 orbits (which we term "a" and "b" for convenience) are actually observed inside the whole kite-shaped region *AEBC* in Fig.6. Each of them is observed , alone, in a larger region. For instance , "a" is observed in between the lines *AD*, *ED'*, and "b" is is observed inbetween *AF* and *CF'* .

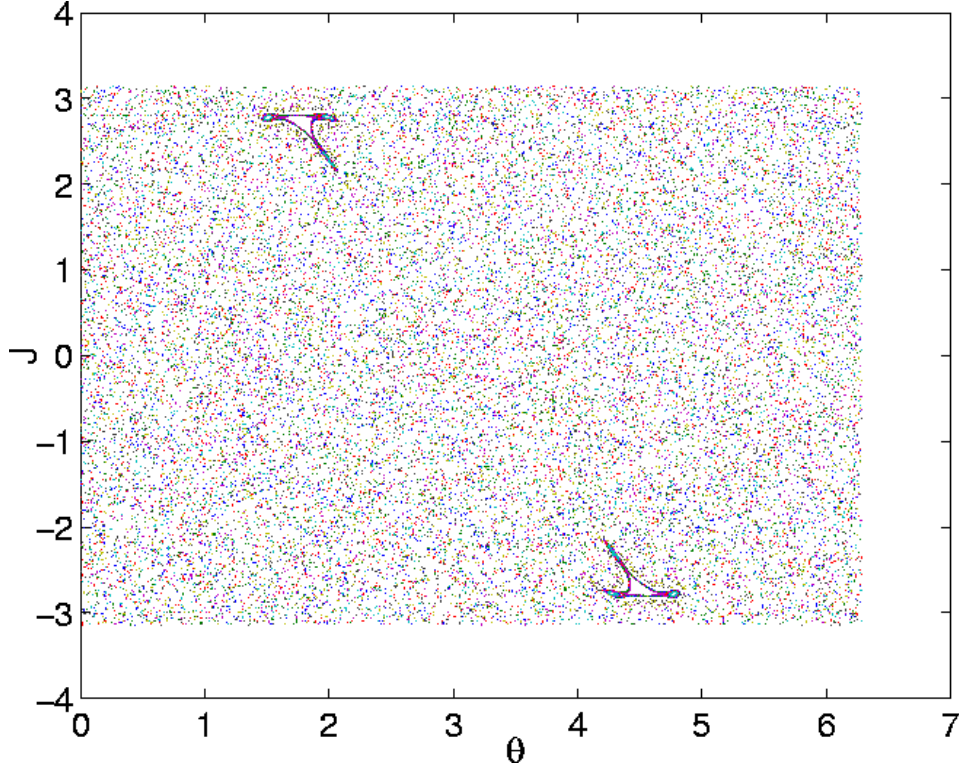


FIG. 4: Phase portrait for $\tilde{k} = 5.5825 > \tilde{k}_s$, and $\Omega = 1$.

On the line AD , "a" coalesces with an unstable orbit and disappears, and "b" disappears in the same way along the line AF . Across the line ED' , "a" bifurcates to a period-4 orbit, and the same happens to "b" across CF' . Resonances of order 3 similar to those found for the $p = 1$ tongue and are presented in Fig. 4 are found also here. As \tilde{k} is increased above the stability border (dot-dashed line in Fig. 5), a period doubling cascade is started. This was studied in the same way as for the $p = 1$ tongue. Results are shown in Table I, and are marked by rhombi and triangles in Figs. 5 and 6.

So far the periodic orbits in the tongue $p = 2, j = 1$ were found identifying one point of the orbit as a fixed point of \mathfrak{J}_B . There is also at least one stable periodic orbit that none of its points are fixed points of \mathfrak{J}_B , but some are fixed points of \mathfrak{J}_A . For $\Omega = 1/2$ one such an orbit of period 4 is $\{X_0 = (0, 0), X_1 = (\pi, 0), X_2 = (0, \pi), X_3 = (\pi, \pi)\}$, as is easily checked. The points X_0 and X_2 are fixed points of \mathfrak{J}_A while X_1 and X_3 are interchanged by this involution. All this demonstrates the Corollary in Appendix A. We checked (by calculating the trace of the tangent map) that the orbit is stable for $0 < \tilde{k} \leq 0.7320$ and $2.7320 \leq \tilde{k} \leq 2.8284$.

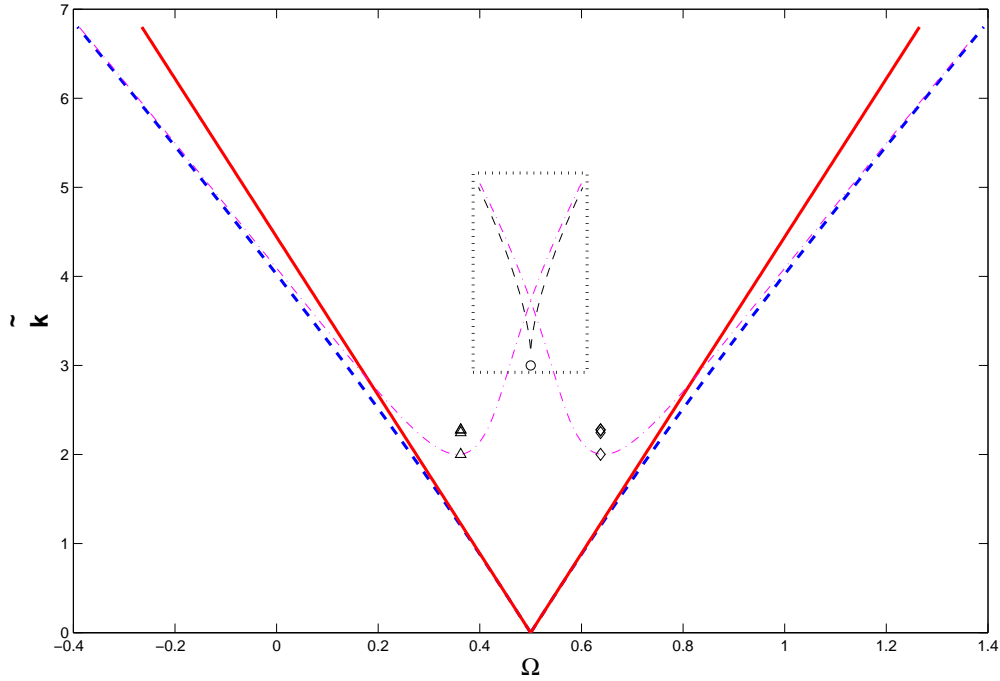


FIG. 5: Phase diagram for the $p = 2$, $j = 1$ tongue. The region of coexistence of two stable periodic orbits of period 2 is framed by the dotted-line rectangle, and zoomed in Fig. 6. The thick dashed lines mark the tongue boundaries (found numerically), and the dash-dotted line is the stability border (found numerically). The solid lines indicate the perturbative analytical result of Eq. (II. 18) for the boundary of the tongue. The small rhombi and triangles indicate the period doubling cascade for $\Omega = 0.6376$ and $\Omega = 0.3624$ correspondingly.

C. The tongue $p = 3$, $j = 1$

Our numerical findings about the $p = 3$, $j = 1$ tongue are summarized by Figs. 8 and 9.

The stable period-3 orbit is lost going upwards across the stability border, the details of which are shown in Figs. 8 and 9. However, a stable such orbit reappears on further increasing \tilde{k} ; it is observed in the region bound by the lines LR and $L'R'$. Between A and B in Fig. 9 there exist two stable periodic orbits of period 3 which we call "a" and "b". Both turn unstable at B . "a" coalesces with an unstable orbit and disappears on the line AD , and "b" disappears in the same way along AF . When crossing CF' , "b" loses stability, and the same happens to "a" along ED' .

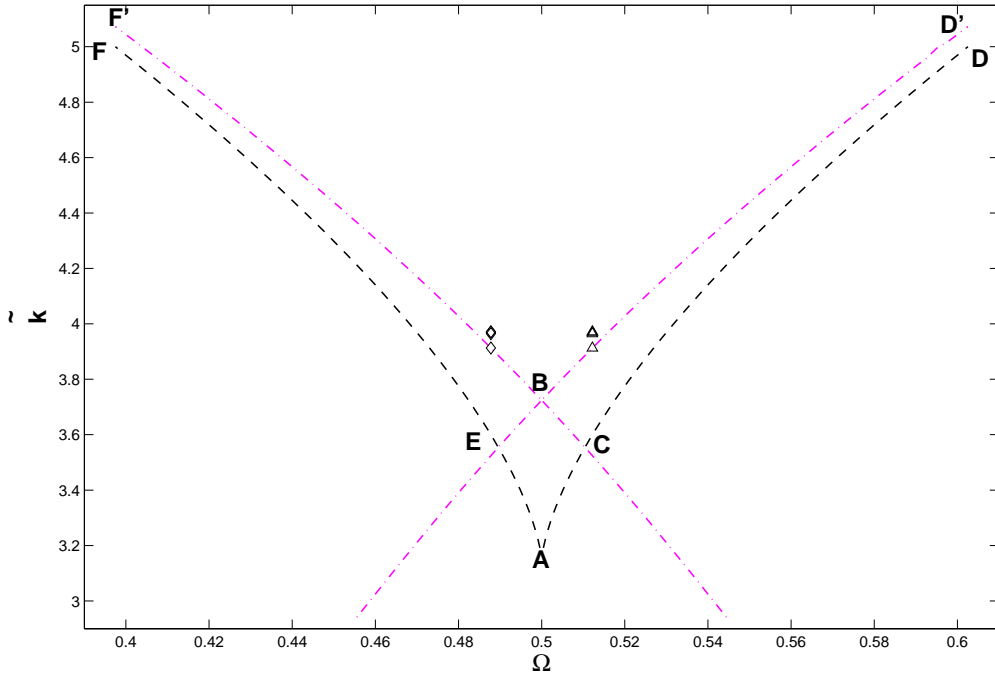


FIG. 6: A zoom-in of the region delimited by the dashed-line rectangle of Fig.5. At the dash-dotted lines period-2 orbits lose stability, and stable period-4 orbits are formed. On the dashed lines coalescence of one of the period-2 orbits with an unstable periodic orbit occurs. This stability loss at the dash-dotted lines is followed by a period doubling cascade. The small rhombi and triangles indicate this cascade for $\Omega = 0.5122$ and $\Omega = 0.4878$ correspondingly.

IV. ORBITS THAT ARE NOT RELATED TO INVOLUTIONS.

In the previous sections periodic orbits that include fixed points of \mathcal{I}_A or \mathcal{I}_B were found. An obvious question is whether periodic orbits can be found, that do not include such fixed points at all. First we find such orbits for $\tilde{k} = 0$. For $\Omega = j/p$, a point (J_0, θ_0) lies in a periodic orbit of period p if $J_0 p + \pi j(p-1) = 2\pi s$ with s integer, and θ_0 is arbitrary, as one can see from (I. 1) and (II. 3). It is easy to find numerically values of j, p, s such that none of the points in such an orbit is fixed under \mathcal{I}_A or \mathcal{I}_B : for instance, with $p = 6$, $j = 3$, and $s = 2$, it is easy to check that none of the fixed-point conditions (II. 6), (II. 7) or (II. 8) is satisfied for any of the points in the periodic orbit. Such an orbit can then be used to find periodic orbits where none of the points is a fixed point of the involutions, also for $\tilde{k} > 0$.

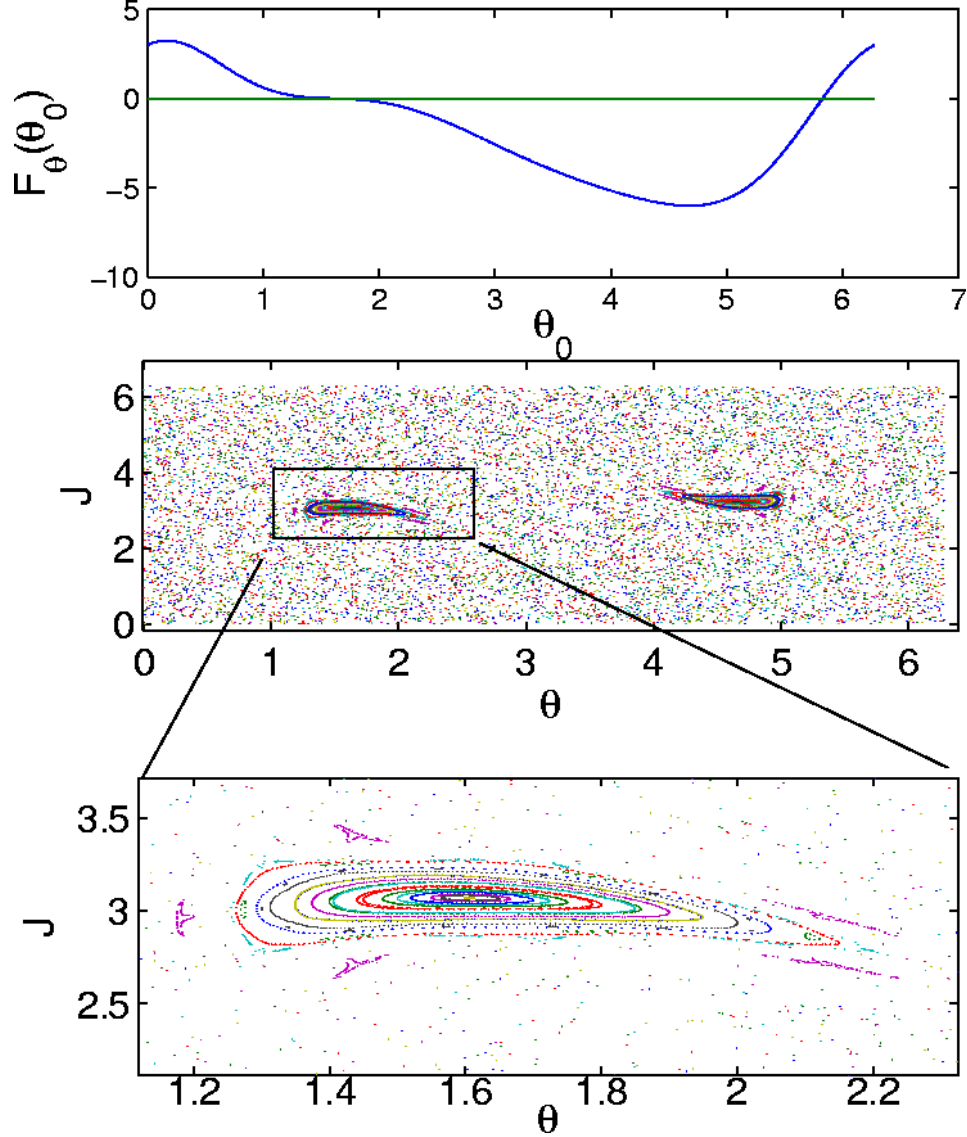


FIG. 7: Phase portrait for $p = 2$, $j = 1$, $\tilde{k} = 3.0$ and $\Omega = 1/2$. The upper slice presents the function $F_\theta(\theta_0)$. The middle slice shows the period two stable orbit and the lower slice is a zoom on one of its island.

For this purpose take $\tilde{k} > 0$ but small. Iterate p times the line of the fixed points of the map with $\tilde{k} = 0$, generating a new line $M^p(J_0, \theta_0)$. Let $(\tilde{J}_0, \tilde{\theta}_0)$ be a point of the intersection of these two lines. Although this is not necessarily a fixed point of M^p for $\tilde{k} > 0$, it is reasonable to look for one in its vicinity, and indeed we found such orbits of period $p = 6$. They are plotted in Fig. 10. These orbits are also related by the symmetry $J \rightarrow -J$ discussed in Appendix B.

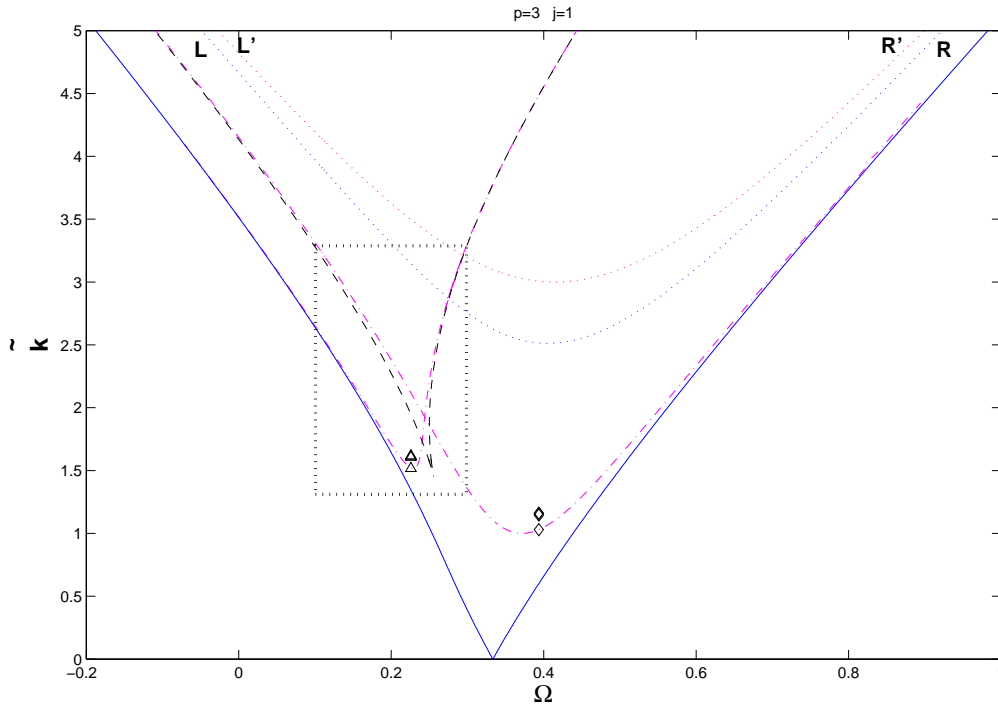


FIG. 8: Phase diagram for the $p = 3$, $j = 1$ tongue, indicating the region of coexistence of two stable period-3 orbits, which is zoomed in Fig. 9. The solid line marks the tongue boundaries found numerically, and the dash-dotted line is the stability border also found numerically. The dashed lines bound the region in which two period-3 orbits coexist. As each of these lines is crossed from the inside of this region, one periodic orbit coalesces with an unstable orbit, and is annihilated. At the stability border a period doubling cascade begins. The rhombi and triangles illustrate such a cascade for $\Omega = 0.3936$ and $\Omega = 0.2285$ correspondingly. Between lines LR and $L'R'$ a stable period 3 orbit is again observed.

V. SUMMARY AND DISCUSSION

In this paper the tongues with $j/p = 1, 1/2, 1/3$ were analyzed in both the perturbative and the nonperturbative regime. A large variety of scenarios for the disappearance of orbits, the loss of their stability and bifurcations was found. We expect similar behavior for the higher order tongues, but the verification is left for further research. For higher values of \tilde{k} some novel results may be found but such an exploration is out of the scope of the present paper.

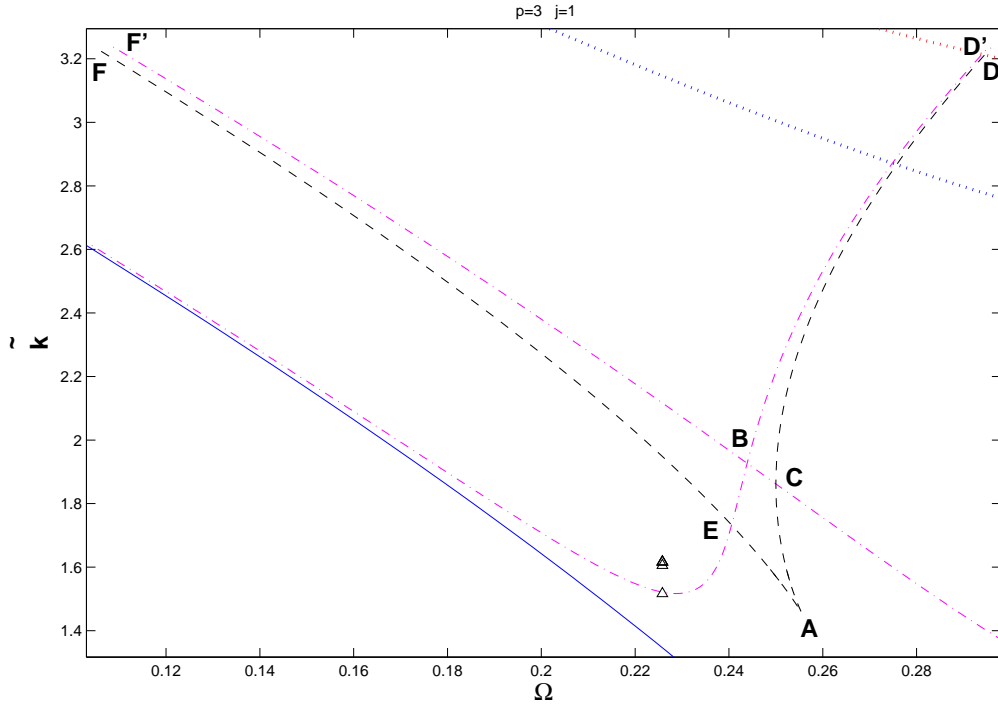


FIG. 9: A zoom-in of the region delimited by the rectangle in Fig. 8.

tongue (p, j)	Ω	\tilde{k}_s	\tilde{k}_∞	α	δ	n_{max}
(1, 0)	0.3692	4.6239	5.1290	-4.0645	8.5839	4
(2, 1)	0.3624	2.0019	2.2790	-3.9919	8.8307	4
(2, 1)	0.6376	2.0019	2.2790	-3.9919	8.8307	4
(2, 1)	0.4878	3.9126	3.9711	-4.0339	8.7034	4
(2, 1)	0.5122	3.9126	3.9711	-4.0339	8.7034	4
(3, 1)	0.3936	1.03	1.1601	-4.1375	8.8534	4
(3, 1)	0.2258	1.5169	1.6167	-4.0315	9.0737	4

TABLE I: As mentioned in the text, the stability of orbits is lost through a period doubling cascade. In this table some examples are given, for different values of Ω .

The research in the present work was confined to the classical regime. The fingerprints of the rich classical behavior that was found on the quantum dynamics in the semiclassical regime may be of great interest. In particular the effect of bifurcations on the eigenstates

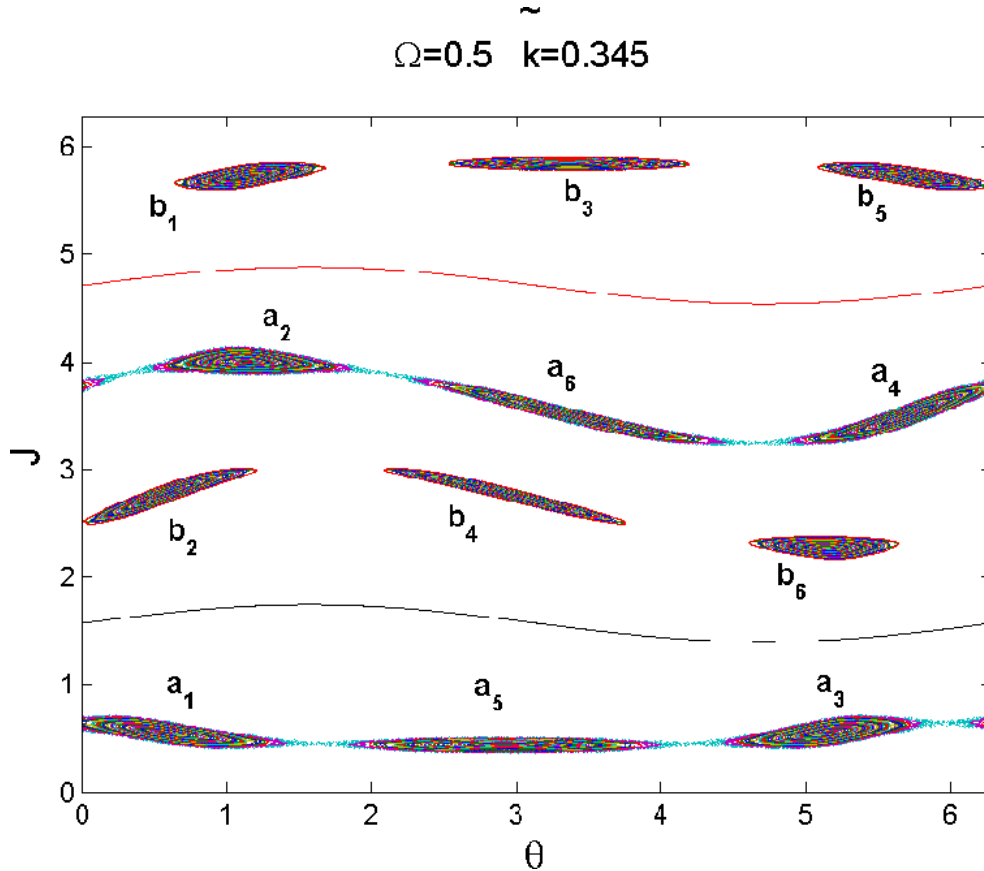


FIG. 10: The two period-6 orbits found at $\Omega = 1/2$ for $\tilde{k} = 0.345$. The two lines indicate the invariant lines under the \mathcal{I}_B involution (as given by (II. 7) and (II. 8)), thus exhibiting that none of the points of these periodic orbits is a fixed point of the \mathcal{I}_B involution. It is also evident that none of the points is a fixed point of \mathcal{I}_A , since none of the points is located on the invariant line of \mathcal{I}_A which is given by (II. 6). Points in one periodic orbit are marked by a_i $i = 1, 2, \dots, 6$ and points in the other by b_i . The involution \mathcal{I}_A transforms the former orbit into the latter, as follows: $a_1 \rightarrow b_1, a_2 \rightarrow b_6, a_3 \rightarrow b_5, a_4 \rightarrow b_4, a_5 \rightarrow b_3, a_6 \rightarrow b_2$, while \mathcal{I}_B transforms them as follows: $a_1 \rightarrow b_2, a_2 \rightarrow b_1, a_3 \rightarrow b_6, a_4 \rightarrow b_5, a_5 \rightarrow b_4, a_6 \rightarrow b_3$. This is a manifestation of theorem 3 of Appendix A.

or the scattering states of the quantum system may reveal novel results. Effects similar to the ones found for quantum ratchets [24] and "flooding" [25] are expected. Also states on islands around periodic orbits related by symmetry may result in states of novel properties. These may lead to effects observable in atom optics experiments.

Acknowledgments

This work was partly supported by the Israel Science Foundation (ISF), by the US-Israel Binational Science Foundation (BSF), by the Minerva Center of Nonlinear Physics of Complex Systems, by the Shlomo Kaplansky academic chair and by the Institute of Theoretical Physics at the Technion. Highly instructive discussions with Roberto Artuso, Andreas Buchleitner, Michael d’Arcy, Simon Gardiner, Shai Haran, Zhao-Yuan Ma, Zeev Rudnick, Gil Summy, are acknowledged. I.G. acknowledges partial support from the MIUR-PRIN project ”Order and Chaos in extended nonlinear systems: coherent structures, weak stochasticity and anomalous transport”.

APPENDIX A: THE INVOLUTION METHOD

This method allows for establishing an analytical relation between the coordinates J, θ of a point on a periodic orbit, and in this way it considerably simplifies the task of computing periodic orbits. The method was introduced by Greene [14] who implemented it in the computation of the approximants of the last bounding KAM trajectory of the Standard Map. In this Appendix the method is reviewed for the reader’s convenience, and its application to the map \mathfrak{M} of (I. 1) is formulated.

Consider a map that can be written as a product of two involutions, i.e.

$$\mathfrak{M} = \mathfrak{I}_2 \mathfrak{I}_1 , \tag{A. 1}$$

where the maps \mathfrak{I}_1 and \mathfrak{I}_2 satisfy $\mathfrak{I}_1^2 = \mathfrak{I}_2^2 = 1$ (the identity map). The following theorems hold:

Theorem 1 *If, for some point X_0 in phase space, and some integer N ,*

$$\mathfrak{I}_1 (X_0) = X_0 , \tag{A. 2}$$

and

$$\mathfrak{I}_1 (\mathfrak{M}^N (X_0)) = \mathfrak{M}^N (X_0) , \tag{A. 3}$$

then

$$\mathfrak{M}^{2N} (X_0) = X_0 . \tag{A. 4}$$

Theorem 2 *If, for some point X_0 in phase space, and some integer N ,*

$$\mathfrak{J}_2 (X_0) = X_0 , \quad (\text{A. 5})$$

and

$$\mathfrak{J}_1 (\mathfrak{M}^N (X_0)) = \mathfrak{M}^N (X_0) , \quad (\text{A. 6})$$

then

$$\mathfrak{M}^{2N+1} (X_0) = X_0 . \quad (\text{A. 7})$$

These theorems are easily proven by explicit use of (A. 2) and (A. 3) in the RHS of (A. 4), and of (A. 5), and of (A. 6) in the RHS of (A. 7).

The opposite direction is not correct. Orbits can be found, such that no point in them is fixed under \mathfrak{J}_1 or \mathfrak{J}_2 (see section IV).

Theorem 3 *Let $\mathcal{O} \equiv \{X_1, X_2, \dots, X_p\}$ be a primitive periodic orbit of period p of the map \mathfrak{M} . For $i = 1, 2$ denote $\mathcal{O}^{(i)} \equiv \mathfrak{J}_i(\mathcal{O})$. Then $\mathcal{O}^{(2)}$ is a primitive periodic orbit of period p , and $\mathcal{O}^{(1)} = \mathcal{O}^{(2)}$.*

Proof: From (A. 1) it follows that $\mathfrak{M}\mathfrak{J}_2 = \mathfrak{J}_2\mathfrak{M}^{-1}$. Therefore, for any $X_j \in \mathcal{O}$,

$$\mathfrak{M}(\mathfrak{J}_2(X_j)) = \mathfrak{J}_2(\mathfrak{M}^{-1}(X_j)) \in \mathfrak{J}_2(\mathcal{O}) = \mathcal{O}^{(2)} , \quad (\text{A. 8})$$

hence $\mathfrak{M}(\mathcal{O}^{(2)}) \subseteq \mathcal{O}^{(2)}$, and then $\mathfrak{M}(\mathcal{O}^{(2)}) = \mathcal{O}^{(2)}$ follows, because \mathfrak{M} is one-to-one. Furthermore, (A. 8) entails that $\mathcal{O}^{(2)}$ is the orbit of any of the points in it, because this is true of \mathcal{O} . Finally,

$$\begin{aligned} \mathcal{O}^{(1)} &= \mathfrak{J}_1(\mathcal{O}) = \mathfrak{J}_1\mathfrak{J}_2\mathfrak{J}_2(\mathcal{O}) \\ &= \mathfrak{J}_1\mathfrak{J}_2(\mathcal{O}^{(2)}) = \mathfrak{M}^{-1}(\mathcal{O}^{(2)}) \\ &= \mathcal{O}^{(2)} . \end{aligned} \quad (\text{A. 9})$$

Theorem 3 has the following direct

Corollary: If in \mathcal{O} there is a fixed point of either involution, then $\mathcal{O} = \mathcal{O}^{(1)} = \mathcal{O}^{(2)}$, and so the orbit is invariant under both involutions. The orbit can be divided in classes such that each class either contains one fixed point of one involution or it contains two points which are mapped onto each other by that involution. In the case when the involution is \mathfrak{J}_A , points

in each such pair have opposite J . For odd p , this implies that a point with $J = 0$ belongs to the periodic orbit (and is a fixed point of \mathfrak{I}_A).

Theorem 1 is employed for finding periodic orbits of even period and Theorem 2 for finding periodic orbits of odd period [14]. One solves for periodic orbits, assuming that in a periodic orbit there is a fixed point X_0 of either \mathfrak{I}_A or \mathfrak{I}_B (in our case, $X_0 = (J_0, \theta_0)$). This assumption reduces the number of unknowns. Since the periodic orbits of \mathfrak{M} and of \mathfrak{M}^{-1} are identical, and $\mathfrak{M}^{-1} = \mathfrak{I}_1 \mathfrak{I}_2$ holds, we can interchange \mathfrak{I}_A and \mathfrak{I}_B in the calculation of periodic orbits. For orbits of odd period one can easily check that $X_0 = (J_0 = 0, \theta_0)$ (eq. II. 6) is a fixed point of \mathfrak{I}_A . In our applications periodic orbits with an odd period p contain a fixed point of \mathfrak{I}_A where (II. 6) is satisfied, while periodic orbits with an even period typically contain a fixed point of \mathfrak{I}_B , where (II. 7) or (II. 8) is satisfied. By the corollary, these orbits must contain more than just 1 fixed point of the latter involution.

APPENDIX B: TIME-REVERSAL SYMMETRY.

In this appendix a symmetry of periodic orbits of \mathfrak{M} is discussed, which is related to time-reversal. The map \mathfrak{M} may be written as $\mathfrak{M} = \mathfrak{M}_K \mathfrak{M}_F$, where

$$\begin{aligned} \mathfrak{M}_F &: (J, \theta) \rightarrow (J, \theta + J), \\ \mathfrak{M}_K &: (J, \theta) \rightarrow (J + \tilde{k} \sin(\theta) + 2\pi\Omega, \theta). \end{aligned} \tag{B. 1}$$

(throughout this appendix, mod 2π is left understood in maps). Let $\mathfrak{M}' \equiv \mathfrak{M}_F \mathfrak{M}_K$. The map \mathfrak{M}' is easily seen to satisfy:

$$\mathfrak{M}^{-1} = \mathfrak{I} \mathfrak{M}' \mathfrak{I}$$

where

$$\mathfrak{I} : (J, \theta) \rightarrow (-J, \theta). \tag{B. 2}$$

and so, denoting $\mathfrak{R} \equiv \mathfrak{I} \mathfrak{M}_F$, the map \mathfrak{R} is an involution: $\mathfrak{R}^2 = 1$, and satisfies

$$\mathfrak{M}^{-1} = \mathfrak{R} \mathfrak{M} \mathfrak{R}. \tag{B. 3}$$

Therefore \mathfrak{R} achieves the time-reversal of the map \mathfrak{M} . We have thus proven that:

Proposition 1 *\mathfrak{M} is time-reversal invariant, in the sense that an area-preserving involution \mathfrak{R} exists, such that $\mathfrak{R} \mathfrak{M} \mathfrak{R} = \mathfrak{M}^{-1}$. Therefore, if \mathcal{O} is a periodic orbit of \mathfrak{M} , then the*

time-reversed orbit $\mathfrak{R}(\mathcal{O})$ is also a periodic orbit of \mathfrak{M} , and the two orbits have the same stability.

Corollary: If for the map (I. 1) there is only one periodic orbit of a given stability (as determined by the tangent map), then $\mathcal{O} = \mathfrak{R}(\mathcal{O})$ must hold, and so for each point in the orbit with momentum J there is another point with the value $-J$.

APPENDIX C: GAUSS SUMS AND PERIODIC ORBITS

In this appendix some properties of Gauss sums that are relevant for the present paper will be reviewed. Specifically we focus on the sum (II. 10), that is related to

$$\tilde{G}(j, p, l) = \frac{1}{p} \sum_{m=1}^p e^{\frac{i\pi}{p}[lm+jm^2]} \quad (\text{C. 1})$$

where in our case $l = j(\chi_p - 1)$ vanishes for even p if (II. 7) holds and it is equal to p if (II. 8) holds while it takes the value $-j$ for odd p . Using elementary calculations one can show [4] that in our case (C. 1) is just (II. 11) divided by p , namely

$$G(j, p) = p\tilde{G}(j, p, l). \quad (\text{C. 2})$$

The calculation of $\xi(j, p)$ is more complicated and will be summarized in what follows. In the standard number theoretical literature ([22] [23]), sums like (C. 1) are calculated for $l = 0$, even j and odd p . Hannay and Berry [20] generalized to other cases of (C. 1) (See also [21]). They show that this sum reduces to the average of the summands and is given, for j and p mutually prime, by Eq. (14) there, which reads:

$$\tilde{G}(j, p, l) = \begin{cases} \frac{1}{\sqrt{p}} \binom{j}{p} \exp \left[-\frac{i\pi}{4}(p-1) - \frac{i\pi j}{p}(j \setminus p)^2 \left(\frac{l}{p}\right)^2 \right] & p \text{ odd, } j \text{ even, } l \text{ even} \\ \frac{1}{\sqrt{p}} \binom{j}{p} \exp \left[-\frac{i\pi}{4}(p-1) - \frac{i4\pi j}{p}(4j \setminus p)^2 l^2 \right] & p \text{ odd, } j \text{ odd, } l \text{ odd} \\ \frac{1}{\sqrt{p}} \binom{p}{j} \exp \left[\frac{i\pi}{4}j - \frac{i\pi j}{p}(j \setminus p)^2 \left(\frac{l}{p}\right)^2 \right] & p \text{ even, } j \text{ odd, } l \text{ even} \end{cases} \quad (\text{C. 3})$$

where $(j \setminus p)$ is the inverse (mod p) of j , notably

$$j(j \setminus p) = 1 \pmod{p} \quad (\text{C. 4})$$

which can be calculated with the help of (whenever j is mutually prime with p):

$$(j \setminus p) = j^{\varphi(p)-1} \pmod{p} \quad (\text{C. 5})$$

where $\varphi(p)$ is Euler's totient function, that is, the number of integers less than p that have no common divisors with p . $\left(\begin{smallmatrix} a \\ b \end{smallmatrix}\right)$ is the Jacobi symbol, where a and b are integers so that b is *odd* and does not divide a . The Jacobi symbol assumes the values ± 1 only, and is the product of the Legendre symbols $\left(\begin{smallmatrix} a \\ q \end{smallmatrix}\right)$ for all the *prime* factors q of b . The Legendre symbol is defined by

$$\left(\begin{smallmatrix} a \\ q \end{smallmatrix}\right) \equiv \begin{cases} 1 & \text{if there is an integer } m \text{ such that } m^2 = a \pmod{q} \\ -1 & \text{if there is no integer } m \text{ such that } m^2 = a \pmod{q} \end{cases} \quad (\text{C. 6})$$

A more straightforward way of determining the value of a Legendre symbol is given by the next formula, which is based on Fermat's little theorem :

$$\left(\begin{smallmatrix} j \\ p \end{smallmatrix}\right) = j^{\frac{p-1}{2}} \pmod{p} \quad (\text{C. 7})$$

keeping in mind that p is an *odd prime* and that j is not divisible by p . For our purposes it is convenient to write the Jacobi symbol in the form

$$\left(\begin{smallmatrix} j \\ p \end{smallmatrix}\right) = \exp \left[\frac{i\pi}{2} \left(1 - \left(\begin{smallmatrix} j \\ p \end{smallmatrix}\right) \right) \right]. \quad (\text{C. 8})$$

It is useful to note that

$$\left(\begin{smallmatrix} -j \\ p \end{smallmatrix}\right) = \left(\begin{smallmatrix} j \\ p \end{smallmatrix}\right) \left(\begin{smallmatrix} -1 \\ p \end{smallmatrix}\right) \quad (\text{C. 9})$$

and that

$$\left(\begin{smallmatrix} -1 \\ p \end{smallmatrix}\right) = e^{\frac{i\pi}{2}(p-1)} \quad (\text{C. 10})$$

and also that

$$\left(\begin{smallmatrix} j \\ 1 \end{smallmatrix}\right) = 1 \quad (\text{C. 11})$$

for all integers j . Other useful formulae are given in appendix B of [20] and in [22] and [23] (see also [21]).

We note that in our case, for even p , $l = 0$ in case (II. 7), and $l = p$ in case (II. 8), while for odd p , $l = -j$. In this case (C. 1) takes the form

$$\tilde{G}(j, p, l) = \frac{1}{\sqrt{p}} e^{i\xi(p, j)} \quad (\text{C. 12})$$

where, for even p corresponding to (II. 7),

$$\xi(p, j) = \frac{\pi}{2} \left[1 - \binom{p}{j} + \frac{j}{2} \right], \quad (\text{C. 13})$$

and for even p corresponding to (II. 8)

$$\xi(p, j) = \frac{\pi}{2} \left[1 - \binom{p}{j} - 2\frac{j}{p}(j \setminus p)^2 \right], \quad (\text{C. 14})$$

while for odd p

$$\xi(p, j) = \begin{cases} \frac{\pi}{2} \left[1 - \binom{j}{p} - \frac{1}{2}(p-1) - \frac{1}{2}\frac{j}{p}(j \setminus p)^2 l^2 \right] & j \text{ even} \\ \frac{\pi}{2} \left[1 - \binom{j}{p} - \frac{1}{2}(p-1) - \frac{8j}{p}(4j \setminus p)^2 l^2 \right] & j \text{ odd} \end{cases} \quad (\text{C. 15})$$

The phase $\xi(p, j)$ determines the relation between θ_0 and ϑ via (II. 13) and can be used to check the accuracy of the calculations. At the center of the tongue $\vartheta = 0$ or $\vartheta = \pi$ while at the boundaries $\vartheta = \frac{\pi}{2}$ or $\vartheta = \frac{3\pi}{2}$. In table II we compare the values of the numerical results $\Delta\theta = \vartheta - \theta_0$ for $\tilde{k} = 0.001$ and θ_0 at the center of some tongues with $\xi(p, j)$ calculated from (C. 13) and (C. 15).

APPENDIX D: A NUMERICAL METHOD FOR THE CALCULATION OF PERIODIC ORBITS

In the numerical solution for periodic orbits we make use of (II. 6), (II. 7) and (II. 8) in order to eliminate J_0 . Then we impose the periodic orbit conditions (II. 4) and require that

tongue (p, j)	$\Delta\theta = \vartheta - \theta_0$	$\xi(p, j)$
(2, 1)	0.7855	$\pi/4 \approx 0.7853$
(3, 1)	0.5235	$\pi/6 \approx 0.5235$
(3, 2)	-0.5235	$-\pi/6 \approx -0.5235$
(4, 1)	0.7855	$\pi/4 \approx 0.7853$
(4, 3)	2.3567	$3\pi/4 \approx 2.3561$
(5, 1)	0.6284	$\pi/5 \approx 0.6283$
(5, 2)	1.2573	$2\pi/5 \approx 1.2566$
(5, 3)	-1.2573	$-2\pi/5 \approx -1.2566$
(5, 4)	-0.6284	$-\pi/5 \approx -0.6283$
(6, 1)	0.7857	$\pi/4 \approx 0.7853$
(6, 5)	-2.3558	$-3\pi/4 \approx -2.3561$
(7, 1)	0.6733	$3\pi/14 \approx 0.6731$
(7, 2)	-0.2251	$-\pi/14 \approx -0.2243$
(7, 3)	2.0209	$9\pi/14 \approx 2.0195$
(7, 4)	-2.0209	$-9\pi/14 \approx -2.0195$
(7, 5)	0.2251	$\pi/14 \approx 0.2243$
(7, 6)	-0.6733	$-3\pi/14 \approx -0.6731$

TABLE II: Numerically computed values of $\Delta\theta = \vartheta - \theta_0$, compared to $\xi(p, j)$ (see (II. 13)).

θ_0 is a common zero of the functions

$$F_J(\theta_0) = \tilde{k} \sum_{n=1}^p \sin \theta_n + 2\pi\Omega p - 2\pi j, \quad (\text{D. 1})$$

where j is determined by the tongue ((II. 4) and (II. 5)), and

$$F_\theta(\theta_0) = pJ_0 + \tilde{k} \sum_{n=1}^p (p-n) \sin \theta_n + \pi\Omega p(p-1) - 2\pi s, \quad (\text{D. 2})$$

that are obtained after iterating the map (I. 1) p times. We solved for zeros of $F_J(\theta_0)$ and $\sin[\frac{1}{2}F_\theta(\theta_0)]$. This is because j is known, while s is unknown and since the function $F_\theta(\theta_0)$ should be taken mod 2π . Then only the common zeros of $F_J(\theta_0)$ and $\sin[\frac{1}{2}F_\theta(\theta_0)]$ are kept. The elimination of J_0 by the involution method, described in Appendix A, reduced

the problem to one of finding zeroes of a function of a single variable, that is a relatively easy task. We used the MATLAB7 routine “fzero” for this purpose [26]. In order to locate the boundary, we note that the zeroes corresponding to the stable and unstable orbits are separated by an extremum of the function in question, say $F_J(\theta_0)$. At the boundary these zeroes coalesce and at this extremum the relevant function vanishes (at the extremum $F_J = 0$). The extremum can be easily found by the MATLAB7 routine “fminbnd” [26]. The boundary of a tongue in the \tilde{k}, Ω space is the locus of points of vanishing extremum. It was found by successive change of \tilde{k} and Ω starting from vertex $\tilde{k} = 0$, $\Omega = j/p$. The boundary was found by the overshoot method, making use of the fact that the value of the function at the extremum changes sign when the boundary of a tongue is crossed.

APPENDIX E: THE RESONANCE OF ORDER 3 FOR THE $p = 1$ TONGUE

When the parameter \tilde{k} is increased across the stability border, the typical scenario of a Hopf bifurcation is observed, with period doubling accompanied by the birth of a resonance of order 3, as shown in Fig. 4. Here we obtain analytical expressions for the first period doubling, and the normal form for the resonance of order 3.

For the map (I. 1) that is studied in the present work, the fixed point (J_0, θ_0) , discussed in subsection III A, loses stability for $\tilde{k}_0 \cos \theta_0 = -4$. In order to analyze the resulting bifurcation, we study the small deviations

$$\begin{aligned}\delta\theta &= \theta - \theta_0 \\ \delta J &= J - J_0.\end{aligned}\tag{E. 1}$$

From (I. 1) we find that to the second order in $\delta\theta$,

$$\begin{aligned}\delta J_{n+1} &= \delta J_n + A\delta\theta_n + D(\delta\theta_n)^2 \\ \delta\theta_{n+1} &= \delta\theta_n + \delta J_{n+1},\end{aligned}\tag{E. 2}$$

where $A = \tilde{k} \cos \theta_0$, $D = -(\tilde{k}/2) \sin \theta_0$. It is convenient to introduce the variable $x = (D/2)\delta\theta$ and turn Eqs. (E. 2) into one second order standard equation (see [3], p. 243)

$$x_{n+1} + x_{n-1} = 2Cx_n + 2x_n^2,\tag{E. 3}$$

where $C = (2 + A)/2$. In our case we are interested in the vicinity of $A = -4$, or $C = -1$. For $C > -1$, the fixed point $x_n = 0$ (corresponding to the original point (J_0, θ_0)) is stable.

For $C < -1$, it becomes unstable and a stable periodic orbit which consists of the points

$$x_{2\pm} = a \pm b, \quad (\text{E. 4})$$

where $a = -(C + 1)/2$ and $b = \frac{1}{2}\sqrt{(C + 1)(C - 3)}$ appears. If $C = -1 - \eta$, then $a = \eta/2$ and $b = \frac{1}{2}\sqrt{\eta(2 + \eta)}$. To study the small deviations, we denote

$$x_n = x_{2\pm} + \Delta x_n, \quad (\text{E. 5})$$

where we numerate the steps so that for even n the point x_n is near x_{2+} , while for odd n it is near x_{2-} . Iterating the map and keeping terms to the second order in the Δx_n , one finds for even n

$$q_{n+2} + q_{n-2} = 2C'q_n + 2q_n^2, \quad (\text{E. 6})$$

where

$$q_n = 2[(C + 2x_{2-}) + (C + x_{2+})^2]\Delta x_n \quad (\text{E. 7})$$

and $C' = -2C^2 + 4C + 7$. In our case $C' = 1 - 8\eta - 2\eta^2$. For odd n the same result is found, but with x_{2-} and x_{2+} interchanged.

The map (E. 6) can be obtained from the Hamiltonian

$$H = \frac{p^2}{2} + V(q) \sum_{n=-\infty}^{\infty} \delta(t - n) \quad (\text{E. 8})$$

with the time rescaled by the factor of 2 and

$$V(q) = -\frac{1}{2}A'q^2 + \frac{2}{3}q^3 \quad (\text{E. 9})$$

with A' related to C' via $C' = (A' + 2)/2$. To see this, one notes that the map obtained from the Hamiltonian (E. 8) is similar to Eq. (E. 2), and therefore, Eq. (E. 6) can be obtained from Eq. (E. 8) in the same way as Eq. (E. 3) is obtained from Eq. (E. 2). The parameter that controls the potential is

$$A' = 2C' - 2 = -4C^2 + 8C + 5 = -16\eta - 4\eta^2. \quad (\text{E. 10})$$

Using the Poisson summation formula we write the periodic δ function in the form $\sum_{n=-\infty}^{\infty} \delta(t - n) = 1 + 2 \sum_{n=1}^{\infty} \cos(2\pi nt)$. For small q the averaged, or time independent, part reduces to a harmonic oscillator with the frequency $\omega = \sqrt{-A'} = 2\sqrt{4\eta + \eta^2}$. The third order resonance is found for $\omega = 2\pi/3$. Introducing the action-angle variables (I, ϕ)

for the linear oscillator part, where $q = \sqrt{2I/\omega} \cos \phi$ and $p = \sqrt{2I\omega} \sin \phi$, the Hamiltonian (E. 8) reads

$$H = \omega I + \frac{4}{3} \left(\frac{I}{2\omega} \right)^{3/2} \cos(3\phi - 2\pi t) + \mathcal{R}(I, \phi, t), \quad (\text{E. 11})$$

where $\mathcal{R}(I, \phi, t)$ is the non-resonant part of the Hamiltonian (E. 8). Introducing the resonant phase $\psi = \phi - 2\pi t/3$ and the detuning from the linear resonance $\delta = \omega - 2\pi/3$, and denoting $r = (4/3)/(2\omega)^{3/2}$ we obtain the normal form for the 3-resonance [27, 28]:

$$H_3 = \delta \cdot I + rI^{3/2} \cos(3\psi). \quad (\text{E. 12})$$

Denoting $\bar{x} = \sqrt{I} \cos(\psi)$, $\bar{y} = \sqrt{I} \sin(\psi)$, we obtain another well known expression for the normal form of the resonance of the order of 3 [27, 28]

$$H_3 = \delta(\bar{x}^2 + \bar{y}^2) + r(\bar{x}^3 - 3\bar{x}\bar{y}^2). \quad (\text{E. 13})$$

As \tilde{k} increases the orbit (E. 4) loses its stability and bifurcates, typically via a period doubling bifurcation cascade.

-
- [1] E.Ott, *Chaos in Dynamical Systems*, Cambridge University Press, Cambridge UK (2002).
 - [2] P.Cvitanovic, R.Artuso, P.Dahlqvist, R.Mainieri, G.Tanner, G.Vattay, N.Whelan, A.Wirzba, *Classical and Quantum Chaos Part I: Deterministic Chaos*, at www.nbi.dk/ChaosBook, version 10.01.06, (2003).
 - [3] A. J. Lichtenberg, M. A. Lieberman, *Regular and stochastic motion*, (Springer, New York, 1983).
 - [4] I. Guarneri, L.Rebuzzi and S. Fishman, *Arnold Tongues and Quantum Accelerator Modes*, quant-ph/0512086, to be published in *Nonlinearity*.
 - [5] S.Fishman, I.Guarneri, and L.Rebuzzi, *Phys.Rev.Lett.* **89**, 084101 (2002).
 - [6] S.Fishman, I.Guarneri, and L.Rebuzzi, *J.Stat.Phys.* **110**, 911 (2003).
 - [7] M. Schell, S. Fraser and R. Kapral, *Phys. Rev. A* **28**, 373 (1983).
 - [8] H.G. Schuster, *Deterministic Chaos, an Introduction* (VCH, Weinheim, 1995).
 - [9] M.H Jensen, P. Bak, and T. Bohr, *Phys. Rev. A* **30**, 1960 (1984).
 - [10] M.B.d'Arcy, G.S.Summy, S.Fishman, and I.Guarneri, *Physica Scripta* **69**, C25 (2004).

- [11] M.K.Oberthaler, R.M.Godun, M.B. D'Arcy, G.S. Summy and K.Burnett, Phys. Rev. Lett. **83**, 4447 (1999); R.M.Godun, M.B.D'Arcy, M.K.Oberthaler, G.S.Summy, and K.Burnett, Phys. Rev. A **62**, 013411 (2000).
- [12] S.Schlunk, M.B.d'Arcy, S.A.Gardiner, and G.S.Summy, Phys. Rev. Lett. **90**, 124102 (2003).
- [13] Z.Y.Ma, M.B. d'Arcy, S.A.Gardiner, Phys. Rev. Lett. **93**, 164101 (2004).
- [14] J.M Greene, J. Math. Phys. **20**, 1183 (1979).
- [15] J.M. Greene, R.S Mackay, F. Vivaldi, M.J. Feigenbaum, Physica 3D, 468 (1981).
- [16] T. Olikar, *Characterization of Periodic Orbits by Topological Considerations for a Kicked Particle*, M.Sc. Thesis, Technion, 2005; T. Olikar and B. Wajnryb to be published.
- [17] J.Farey, *On a Curious Property of Vulgar Fractions*, London, Edinburgh and Dublin Phil.Mag **47**, 385 (1816). See, however, a historical note in ref.[18], p.36.
- [18] G.H.Hardy and E.M.Wright, Ch.3 in *An Introduction to the Theory of Numbers*, 5th ed., Oxford, England: Clarendon press, (1979).
- [19] I.Niven and H.S.Zuckerman, *An Introduction to the Theory of Numbers*, (Wiley, N.Y., 1960).
- [20] J.H.Hannay and M.V.Berry, Physica D **1**, 267 (1980).
- [21] M.V.Berry and S.Klein, J. Mod. Opt **43**, 2139 (1996) and M.V.Berry and E.Bodenschatz , J. Mod. Opt **46**, 349 (1999)
- [22] S. Lang, Algebraic Number Theory (Addison-Wesley, New York, 1970).
- [23] P.G.L. Dirichlet with supplements by R. Dedekind, *Lectures on number theory, History of mathematics*; v. 16, (American mathematical society, 1999).
- [24] T.S. Monteiro, P.A. Dando, N. Hutchings, M. Isherwood, Phys.Rev.Lett. **89**, 194102 (2002); T. Jonckheere, M. Isherwood and T.S. Monteiro Phys.Rev.Lett. **91**, 253003 (2003); P.H. Jones, M. Goonasekera, H.E. Saunders-Singer, T.S. Monteiro, D.R. Meacher, preprint (physics/0504096).
- [25] R.Ketzmerick, and A.G.Monastra, Phys. Rev. Lett. **94**, 054102 (2005).
- [26] MATLAB7 User-guide.
- [27] V.I. Arnol'd, *Mathematical methods of classical mechanics*, (New York, Springer, 1989).
- [28] V.V. Kozlov, A.I. Neishtadt, and V.I. Arnold, *Mathematical aspects of classical and celestial mechanics*, (Springer, Berlin, 1997).